

Bi₄Br₄-based saturable absorber with robustness at high power for ultrafast photonic device

Wenjun Liu,^{1,3} Xiaolu Xiong,^{2,4} Mengli Liu,¹ XiaoWei Xing,¹ Hailong Chen,³
Han Ye,¹ Junfeng Han,^{2,4,a} and Zhiyi Wei^{3,a}

¹ State Key Laboratory of Information Photonics and Optical Communications, School of Science, P. O. Box 91, Beijing University of Posts and Telecommunications, Beijing 100876, China

² Centre for Quantum Physics, Key Laboratory of Advanced Optoelectronic Quantum Architecture and Measurement (MOE), School of Physics, Beijing Institute of Technology, Beijing, 100081, China.

³ Beijing National Laboratory for Condensed Matter Physics, Institute of Physics, Chinese Academy of Sciences, Beijing 100190, China

⁴ Yangtze Delta Region Academy of Beijing Institute of Technology, Jiaxing, 314000, China

^a Authors to whom correspondence should be addressed: pkuhjf@bit.edu.cn and zywei@iphy.ac.cn

Saturable absorption may be induced at critical pumping power by the nonlinear optical effects of nanomaterials, thereby making it possible to generate high-power ultrafast laser. Recently, the Bi₄Br₄ is theoretically predicted to be a member of topological insulators, and is expected to be the promising candidate for saturable absorbers (SAs). We show here that Bi₄Br₄ features large modulation depth of 42.3%. The Bi₄Br₄-based SA enables mode-locking operation at near-infrared range, as demonstrated here by a 1.5 μm fiber laser with signal-to-noise ratio (SNR) of 90 dB and pulse duration of 172 fs. Moreover, the robustness of the Bi₄Br₄-based SA at relatively high power is of particular interest, which can be proved by the laser's stable operation state. The strong optical nonlinearity and robustness provided by Bi₄Br₄ may arouse a growing upsurge in the innovation of high-power ultrafast photonic devices and further development of photon applications.

Ultrafast lasers afford high pulse instantaneous intensity, repetition rate, temporal and spatial resolution, which are essential in the research of laser microsurgery, bioimaging, large-capacity optical communication and high-precision material processing¹⁻⁶. After years of development, the mature passively mode-locking technology has been considered to be one of the most effective technologies in the formation of ultrafast pulses⁷⁻¹¹. The core of this technology is the nonlinear optical (NLO) modulation device, which exhibits absorption saturation owing to its nonlinear interaction with light and is often called the saturable absorber (SA)¹². So far, this kind of absorption saturation involving fast relaxation of valence or conductive electrons has been observed in various materials¹³⁻¹⁶. Generally speaking, ideal saturable absorber is expected

This is the author's peer reviewed, accepted manuscript. However, the online version of record will be different from this version once it has been copyedited and typeset.

PLEASE CITE THIS ARTICLE AS DOI: 10.1063/1.50077148

to have narrow band gap for broadband applications, strong nonlinearity and fast relaxation time for effective pulse narrowing. Therefore, the nanomaterials with low dimensional structure have become the main choice due to their excellent photoelectric properties¹⁷⁻²⁰. For instance, gapless materials graphene, exhibits ultrafast carrier relaxation process, high damage threshold and broadband absorption in the application of lasers. At the same time, the narrow band gap means that the material can realize the application of higher band mode-locked fiber laser²¹. The narrow band gap materials have some excellent research results around 2 μm band²². Most of the valued properties are attributed to its Dirac cone structure. On the one hand, as the density of states is small, it is easy to achieve saturation absorption. On the other hand, the carrier relaxation speed is fast in this structure, which is conducive to the construction of ultrafast fiber laser. However, the absorption of single-layer graphene is limited, which will affect the efficiency of laser output²³. Although the multilayer graphene can enhance the absorption of light, it can inevitably bring loss, which affects the performance such as output power of the laser²⁴.

In recent years, a kind of graphene-like Dirac material called topological insulator (TIs) with narrow band-gap and metallic surface or edge states have aroused a worldwide research upsurge²⁵. As the band gap of TIs is small, the applicable spectral range can be extended to mid-infrared. Meanwhile, the surface state with Dirac cone can enhance its relaxation speed fast²⁶. Therefore, it has great potential in saturable absorption. Due to the excellent strong optical nonlinearity and broadband saturable absorption, TIs have been regarded as another promising and powerful candidate for ultrafast pulse generation²⁷. Recently, the Bi_4Br_4 is theoretically predicted to be a member of topological insulators, and is expected to be the promising candidate for multichannel dissipationless electronic devices²⁸⁻²⁹. The bandgap of monolayer Bi_4Br_4 is reported to be ~ 0.2 eV with gapless edge states³⁰⁻³¹, which indicates that it has the potential to exhibit absorption properties in the near infrared and even wider range.

In this contribution, the nonlinear optical properties of Bi_4Br_4 have been specifically investigated through experiments. The Bi_4Br_4 SA is prepared via a self-flux method³², which is an effective method to grow crystal materials. Before being applied to the laser, the Bi_4Br_4 SA is found to exhibit an attractive nonlinear absorption, the saturation intensity and

This is the author's peer reviewed, accepted manuscript. However, the online version of record will be different from this version once it has been copyedited and typeset.

PLEASE CITE THIS ARTICLE AS DOI: 10.1063/1.50077148

modulation depth of which are 0.55 MW/cm^2 and 42.3%, respectively. Further, the laser integrated with the Bi_4Br_4 SA has been demonstrated to produce ultrafast pulses with pulse duration of 172 fs. The SNR up to 90 dB and output power of 20 mW illustrate the stability of the Bi_4Br_4 SA in continuous operation at high power. The excellent performance of Bi_4Br_4 as a SA in laser illustrates its potential value in expanding effective nonlinear photonic devices, which may bring down to the further practical application of Bi_4Br_4 and the innovation of ultrafast photons.

FIG. 1(a)-1(c) illustrate morphology and three-dimensional image of Bi_4Br_4 , respectively. The typical line profile is shown in FIG. 1(b), which shows that the material has a thickness of about 200 nm. Most of area on top surface are flat along with several steps at the edge. The topography of Bi_4Br_4 were recorded by scanning electron microscope (SEM), as shown in FIG. 1(d). The element mapping of Br and Bi are shown in FIG. 1(e) and 1(f). The energy dispersive X-ray spectrum in FIG. 1(g) reveals the peak of atom Bi, Br, Si, O, and Si, O originates from substrates. The actual composition of the sample listed in figure 1 indicates that Bi/Br atomic ratio is 1:1.

In FIG. 2, the Bi_4Br_4 flakes and SA are characterized. The bright-field transmission electron microscopy (TEM) image of Bi_4Br_4 flake is shown in FIG. 2(a). The flake is continuous and homogeneous in a large scale. FIG. 2(b) shows a high-resolution image of the Bi_4Br_4 crystal lattice. The measured lattice distance from the TEM image is 4.2 \AA , corresponding to a direction of Bi_4Br_4 single crystals in FIG. 2(c). Then, the x-ray diffraction (XRD) peaks were collected as shown in FIG. 2(d). The main diffraction peaks can be indexed as the (00l) reflections of $\alpha\text{-Bi}_4\text{Br}_4$, suggesting that the measured plane is the ab plane.

The power-dependent nonlinear transmission of the Bi_4Br_4 -based SA is measured by a mode-locked fiber laser (MLFL) featuring a repetition rate of 120 MHz and a pulse duration of 700 fs at $1.5 \mu\text{m}$. The measured data in FIG. 2(e) are fitted by a widely accepted standard two-level saturable absorber model. With 800 nm excitation light and $5 \mu\text{m}$ probe light, we get the experimental data as shown in the orange dot in FIG. 2(f). After performing a fitting analysis with the multiple-exponential functions, the relaxation is decomposed into two decay components: an ultrafast component with characteristic time of 200 fs and a fast component with characteristic time of 3.2 ps. As the photon energy of pump and

This is the author's peer reviewed, accepted manuscript. However, the online version of record will be different from this version once it has been copyedited and typeset.

PLEASE CITE THIS ARTICLE AS DOI: 10.1063/5.0077148

probe light are larger than the band gap of Bi₄Br₄ (0.2 eV), both of them can cause inter-band transfer of electrons.

The balanced twin-detector method can be shown in FIG. 3(a). The modulation depth, saturation intensity and non-saturable absorption loss of the Bi₄Br₄ SA are measured by this method³². The pulse source is a homemade 125 MHz fiber laser centered at 1550 nm with 100 fs pulse duration and 80 mW output power. A variable optical attenuator (VOA) is used to control the power level of the optical pulses. A 50:50 optical coupler (OC) is applied to dividing the incident optical pulses into two paths with the same power. The main function of the circulator is to pass optical pulses through the SA mirror with a spatial structure. By rotating the VOA, we can measure the different output powers from high to low at two detectors. Based on the measured data, we can fit the saturable absorption of the Bi₄Br₄ SA, as described by the model:

$$\alpha(I) = \frac{\alpha_s}{1 + I/I_{sat}} + \alpha_{ns},$$

where α_s is the modulation depth (saturable loss), α_{ns} is the nonsaturable loss, and I_{sat} is the saturable intensity. The performance difference of transmission rate under different power presents a modulation depth (α_s) of 42.3%, meanwhile, the saturable intensity (I_{sat}) and nonsaturable loss (α_{ns}) are assessed as 0.55 MW/cm² and 26.4%, respectively. The modulation depth of the Bi₄Br₄-based SA higher than other saturable materials reveals the strong nonlinearity of Bi₄Br₄ and its potential as a modulation device. Small insertion loss of 1.3 dB is also acceptable for its further laser applications. The time-resolved pump-probe profiles of Bi₄Br₄ are obtained using a femtosecond laser system³³. Such set up of the pump-probe analyses can help us to understand the decay process related with inter-band recombination in Bi₄Br₄ in FIG. 3(b). There, we can assume that the response time is sufficient as an ultrafast saturated absorber.

Inspired by the research of the MLFL near 2 μ m, we predict that Bi₄Br₄ has the potential to exhibit absorption characteristics in near infrared or even wider range³⁴. By the notable saturable absorption properties previously shown, it is quite promising to establish the mode-locked laser using the Bi₄Br₄-based SA. The experimental schematic diagram of ring cavity laser employing the Bi₄Br₄-based SA is displayed in FIG. 4(a). A laser diode (LD) operating at 980 nm is to pump the 0.5 m long gain medium commercial erbium doped fiber (EDF) via a 980/1550 nm wavelength-division multiplexer (WDM). The function of the polarization controller (PC) is to alter the polarization state of light to optimize

This is the author's peer reviewed, accepted manuscript. However, the online version of record will be different from this version once it has been copyedited and typeset.

PLEASE CITE THIS ARTICLE AS DOI: 10.1063/1.50077148

the working state. To implement the operation of unidirectional travelling, an isolator (ISO) is integrated into the laser cavity. 20% of the laser light are extracted from the cavity via a fiber optical coupler (OC) for real-time observation and measurement. In order to avoid the measurement error caused by different samples, only one flake is used during the experiment in the fiber laser. The flakes, which are exfoliated from the same single crystal with the same thickness, are used in the measurement of the saturable absorption and pump-probe. The pulse sequence is monitored in real time by an oscilloscope (Tektronix DPO 3054), the autocorrelator (APE Pulse check), optical spectrum analyzer (Yokogawa AQ 6370C) and RF spectrum analyzer (Rohde& Schwarz FSW26) are used for further measurement of the acquired mode-locked signals.

By properly adjusting the pump power and fine-tuning the PC, a mode-locking phenomenon is observed on the oscilloscope at the pump power of 234 mW. The time interval between two pulses in FIG. 4(b) is 20 ns, which is in good agreement with the repetition frequency of 49.92 MHz. FIG. 4(c) illustrates the optical spectrum of mode-locking centered at 1559.23 nm and shows a 3-dB bandwidth about 23.26 nm. To the naked eye, the spectra sampled every four hours maintain good consistency in shape. FIG. 4(d) presents the first peak of radio frequency (RF) spectrum appearing at 49.92 MHz. By comparing the maximum value of the peak and the background value, the SNR is calculated to be 90 dB. The RF sequences in the illustration are uniformly arranged without spectral modulation over a wide range, indicating the well operation of laser. Long-term spectrum monitoring and high SNR make us confident of the stability of this mode-locked system. The autocorrelation trace is recorded in FIG. 4(e). The soliton generated in the laser is generally approximated as hyperbolic secant. As a result, the curve fitting the experimental data with Sech^2 intensity profile reveals a pulse duration of 172 fs.

To investigate the performance of the Bi_4Br_4 -based SA at high power, the pump power is controlled within a suitable range. In the process of gradually increasing the pump power from 234 mW to 630 mW, the intensity of the mode-locked sequences measured by the power meter is significantly increased as shown in FIG. 4, which indicates that the mode-locking laser shows superior robustness. Due to the higher pump power (630 mW) and lower nonsaturable loss (26.4%),

the final output power of the MLFL is recorded as 20 mW.

Table 1 Comparison of ultrafast MLFLs based on some materials.

Materials	α_s^a	λ^b (nm)	τ^c (fs)	f_{rep}^d (MHz)	P_{pump}/P_{out} (mW)	Efficiency	Refs.
Graphene	65.9%	1561	1230	2.54	120/3	2.5%	24
Bi ₂ Se ₃	3.9%	1557.5	660	12.5	90/1.8	2%	35
Bi ₂ Te ₃	15.7%	1547	600	15.11	55/0.8	1.6%	36
BP	4.6%	1560.5	272	28.2	65/0.5	0.8%	37
MoS ₂	2.7%	1556.3	606	463	287/5.9	2%	38
WS ₂	2.9%	1572	595	25	310/4	1.3%	39
MoSe ₂	0.63%	1558.25	1450	8	50/0.4	0.8%	40
WTe ₂	2.85%	1556.2	770	13.98	25/0.04	0.2%	41
Bi ₄ Br ₄	42.3%	1559.23	172	49.92	630/20	3.2%	This work

Moreover, the relationship curve between pump power and output power shows almost constant slope, and no signal of fading is observed in the later stages of high power as shown in FIG. 4(f). Hence, one can see that the Bi₄Br₄-based SA is expected to maintain stable nonlinear absorption at higher powers. Further, the long-term jitter of the laser at the highest pump power is monitored at a frequency of once per second as shown in FIG. 4(g). During 16 hours of monitoring, the output power jitter is 0.59 mW, and the corresponding dispersion is 2.9%, indicating the durable and reliable effectiveness of the Bi₄Br₄ SA.

After referring to the performance comparison in Table 1, the laser employing the Bi₄Br₄-based SA does not seem to be inferior to the laser based on other materials. The Bi₄Br₄-based SA features the large modulation depth of 42.3%. The pulse duration of 172 fs obtained from the mode-locked laser highlights the potential of the Bi₄Br₄-based SA in the realization of ultrafast pulses. From the values of pump power and output power of various lasers in Table 1, the conversion rate in power of the Bi₄Br₄-based laser is decent. It is worth mentioning that it withstands higher pump power than other materials. Therefore, its durability at high power is worthy of recognition.

In conclusion, the optical nonlinearity of Bi₄Br₄ has been experimentally investigated here by a pulsed laser. The Bi₄Br₄-based SA has featured the large modulation depth of 42.3%, and played a key role in the realization of mode-locked laser. The implemented mode-locked laser at 1559.23 nm has been characterized by a repetition frequency of 49.92 MHz, a SNR of 90 dB and a pulse duration of 172 fs, respectively. Besides, the Bi₄Br₄-based SA has indicated a strong resistance

This is the author's peer reviewed, accepted manuscript. However, the online version of record will be different from this version once it has been copyedited and typeset.

PLEASE CITE THIS ARTICLE AS DOI: 10.1063/1.50077148

to the relatively high pump power and maintained robustness under long-term high-power excitation. The potential of Bi₄Br₄ in the development and innovation of nonlinear optics and ultrafast photonic devices operating in the near infrared and wider bands deserves to be focused and further explored.

This work was financially supported by Beijing Natural Science Foundation (JQ21019); the National Natural Science Foundation of China (11875008, 11734003, 12075034); the National Key Research and Development Program of China (2020YFA0308800); the Open Research Fund of State Key Laboratory of Pulsed Power Laser Technology (Grant SKL2019KF04); Fundamental Research Funds for the Central Universities (2019XD-A09-3).

AUTHOR DECLARATIONS

Conflict of Interest

The authors report no conflicts of interest.

DATA AVAILABILITY

The data that support the findings of this study are available from the corresponding author upon reasonable request.

References.

- ¹U. Keller, *Nature* **424**, 831 (2003).
- ²J. Su, L. Chai, W. Liu, and M. Hu, *IEEE J. Quantum Electron.* **55**, 1 (2019).
- ³A. H. Zewail, *Science* **242**, 1645 (1998).
- ⁴S. D. Jackson, *Nat. Photonics* **6**, 423 (2012).
- ⁵R. R. Gattass, and E. E. Mazur, *Nat. Photonics* **2**, 219 (2008).
- ⁶C. Xu, and F. W. Wise, *Nat. Photonics* **7**, 875 (2013).
- ⁷M. L. Liu, W. J. Liu, and Z. Y. Wei, *J. Lightwave Technol.* **37**, 3100 (2019).
- ⁸R. Y. Liao, Y. J. Song, and M. L. Hu, *Opt. Express* **27**, 14705 (2017).
- ⁹Y. W. Zhao, J. T. Fan, H. S. Shi, Y. P. Li, Y. J. Song, and M. L. Hu, *Opt. Express* **27**, 8808 (2019).
- ¹⁰W. Liu, R. Y. Liao, J. Zhao, J. H. Cui, Y. J. Song, C. Y. Wang, and M. L. Hu, *Optica* **6**, 194 (2019).
- ¹¹Y. I. Jhon, J. Koo, B. Anasori, M. Seo, J. H. Lee, Y. Gogotsi, and Y. M. Jhon, *Adv. Mater.* **29**, 1702496 (2017).
- ¹²W. J. Liu, M. L. Liu, Y. Y. Ouyang, H. R. Hou, and Z. Y. Wei, *Nanotechnology* **29**, 394002 (2018).
- ¹³T. Jiang, K. Yin, C. Wang, J. You, H. Ouyang, and R. Miao, *Photonics Res.* **8**, 78 (2020).
- ¹⁴H. Zhang, D. Y. Zhao, L. M. Zhao, Q. L. Bao, and K. P. Loh, *Opt. Express* **17**, 17630 (2009).
- ¹⁵Z. Q. Luo, Y. Z. Huang, M. Zhong, Y. Y. Li, J. Y. Wu, B. Xu, H. Y. Xu, Z. P. Cai, J. Peng, and J. Weng, *J. Lightwave Technol.* **32**, 4077 (2014).
- ¹⁶M. Zhang, G. H. Hu, G. Q. Hu, R. C. T. Howe, L. Chen, Z. Zheng, and T. Hasan, *Sci. Rep.* **5**, 11453 (2015).
- ¹⁷R. L. Miao, Z. W. Shu, Y. Z. Hu, Y. X. Tang, H. Hao, J. You, X. Zheng, X. A. Cheng, H. G. Duan, and T. Jiang, *Opt. Lett.* **44**, 3198 (2019).
- ¹⁸C. X. Zhang, H. Ouyang, R. L. Miao, Y. Z. Sui, H. Hao, Y. X. Tang, J. You, X. Zheng, Z. J. Xu, X. A. Cheng, and T. Jiang, *Adv. Opt. Mater.* **7**, 1900631 (2019).
- ¹⁹W. J. Liu, L. H. Pang, H. N. Han, K. Bi, M. Lei, and Z. Y. Wei, *Nanoscale* **9**, 5806 (2017).

This is the author's peer reviewed, accepted manuscript. However, the online version of record will be different from this version once it has been copyedited and typeset.

PLEASE CITE THIS ARTICLE AS DOI: 10.1063/1.50077148

- ²⁰W. J. Liu, M. L. Liu, H. N. Han, S. B. Fang, H. Teng, M. lei, and Z. Y. Wei, *Photonics Res.* **6**, C15 (2017).
- ²¹M. Jung, J. Lee, J. Park, J. Koo, Y. M. Jhon, and J. H. Lee, *Opt. Express* **23**, 19996 (2015).
- ²²J. Lee, Y. I. Jhon, K. Lee, Y. M. Jhon, and J. H. Lee, *Sci. Rep.* **10**, 15305 (2020).
- ²³E. G. Mishchenko, *Phys. Rev. Lett.* **103**, 246802 (2009).
- ²⁴Q. L. Bao, H. Zhang, Z. H. Ni, Y. Wang, L. Polavarapu, Z. X. Shen, Q. H. Xu, D. Y. Tang, and K. P. Loh, *Nano Res.* **4**, 297 (2011).
- ²⁵M. Z. Hasan, and C. L. Kane, *Rev. Mod. Phys.* **82**, 3045 (2010).
- ²⁶P. G. Yan, R. Y. Lin, S. C. Ruan, A. J. Liu, and H. Chen, *Opt. Express* **23**, 154 (2015).
- ²⁷H. J. Zhang, C. X. Liu, X. L. Qi, X. Dai, Z. Fang, and S. C. Zhang, *Nat. Phys.* **5**, 438 (2009).
- ²⁸C. H. Hsu, X. T. Zhou, Q. Ma, N. Gedik, A. Bansil, V. M. Pereira, H. Lin, L. Fu, S. Y. Xu, and T. R. Chang, *2D Mater.* **6**, 031004 (2019).
- ²⁹J. J. Zhou, W. Feng, G. B. Liu, and Y. Yao, *Nano Lett.* **14**, 4767 (2014).
- ³⁰X. Li, D. Chen, M. Jin, D. Ma, and Y. Yao, *P. Natl. Acad. Sci.* **116**, 17696 (2019).
- ³¹J. J. Zhou, W. X. Feng, C. C. Liu, S. Guan, and Y. G. Yao, *New J. Phys.* **17**, 015004 (2015).
- ³²W. J. Liu, M. L. Liu, X. Chen, T. Shen, M. Lei, J. G. Guo, H. X. Deng, W. Zhang, C. Q. Dai, X. F. Zhang, and Z. Y. Wei, *Commun. Phys.* **3**, 15 (2020).
- ³³Y. Terada, S. Yoshida, O. Takeuchi, and H. Shigekawa, *J. Phys.-Condens. Mat.* **22**, 264008 (2010).
- ³⁴Y. I. Jhon, J. Lee, Y. M. Jhon, and J. H. Lee, *IEEE J. Sel. Top. Quant.* **24**, 1102208 (2018).
- ³⁵H. Liu, X. W. Zheng, M. Liu, N. Zhao, A. P. Luo, Z. C. Luo, W. C. Xu, H. Zhang, C. J. Zhao, and S. C. Wen, *Opt. Express* **23**, 27503 (2015).
- ³⁶J. Lee, J. Koo, Y. M. Jhon, J. H. Lee, *Opt. Express* **22**, 6165 (2014).
- ³⁷J. Sotor, G. Sobon, W. Macherzynski, P. Paletko, and K. M. Abramski, *Appl. Phys. Lett.* **107**, 051108 (2015).
- ³⁸K. Wu, X. Y. Zhang, J. Wang, and J. P. Chen, *Opt. Lett.* **40**, 1374 (2015).
- ³⁹K. Wu, X. Y. Zhang, J. Wang, X. Li, and J. P. Chen, *Opt. Express* **23**, 11453 (2015).
- ⁴⁰Z. Q. Luo, Y. Y. Li, M. Zhong, Y. Z. Huang, X. J. Wan, J. Peng, and J. Weng, *Photonics Res.* **3**, A79 (2015).
- ⁴¹J. Koo, Y. I. Jhon, J. Park, J. Lee, Y. M. Jhon, and J. H. Lee, *Adv. Funct. Mater.* **26**, 7454 (2016).

This is the author's peer reviewed, accepted manuscript. However, the online version of record will be different from this version once it has been copyedited and typeset.

PLEASE CITE THIS ARTICLE AS DOI: 10.1063/1.50077148

FIGURE CAPTIONS

FIG. 1 The AFM, SEM and EDS of Bi_4Br_4 nanobelt. (a) Topography of exfoliated Bi_4Br_4 recorded in scanasyst mode. (b) AFM height profile taken along the green line in (a). (c) 3D image of exfoliated Bi_4Br_4 . (d) SEM of exfoliated Bi_4Br_4 . (e) The element mapping of Br. (f) The element mapping of Bi. (g) EDS spectrum of Bi_4Br_4 .

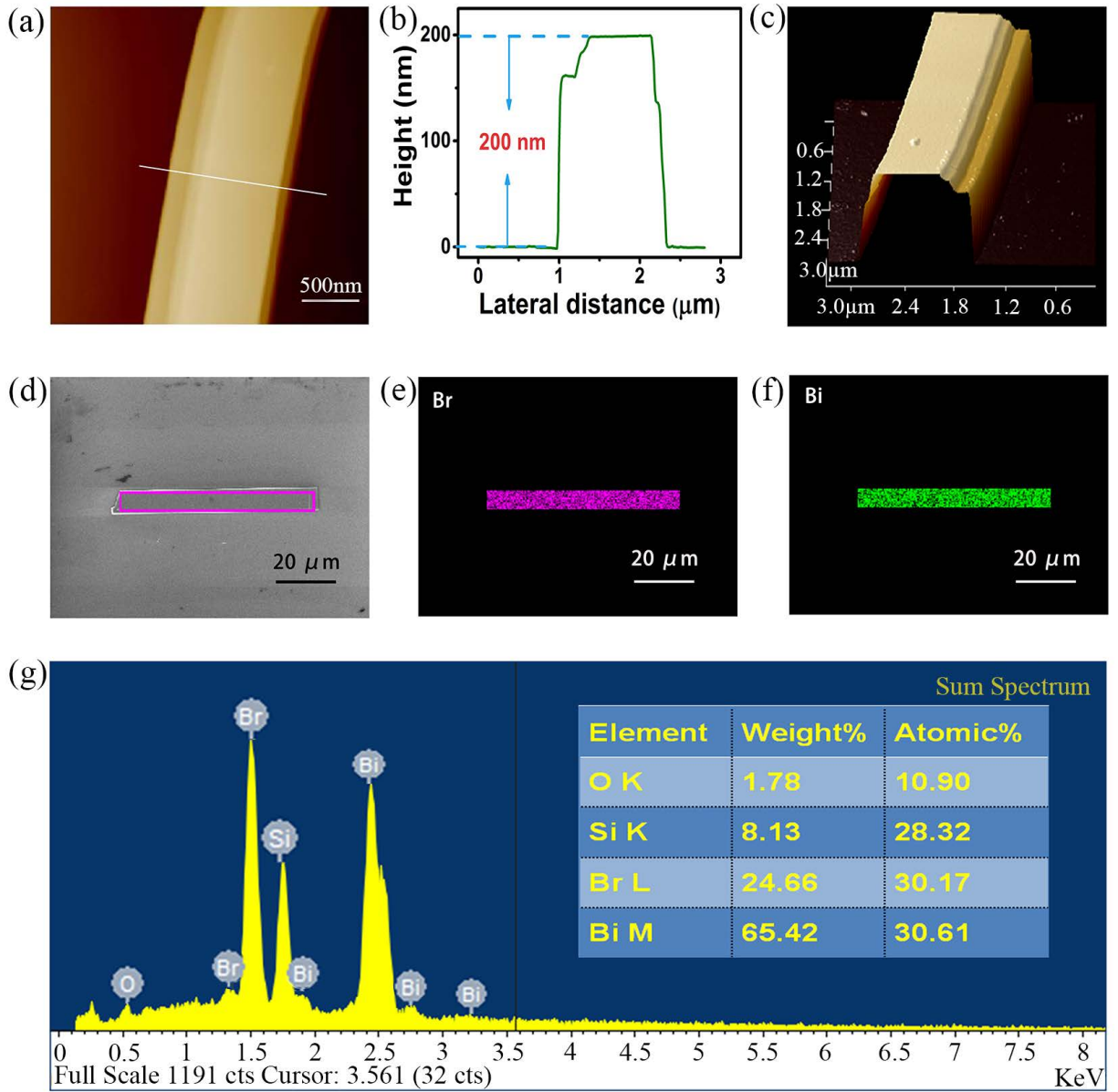
FIG. 2 The TEM, XRD and nonlinear transmission of the Bi_4Br_4 flakes from the same single crystal. (a) Bright field TEM image of $\alpha\text{-Bi}_4\text{Br}_4$ nanobelt. (b) High resolution TEM image obtained from the top of $\alpha\text{-Bi}_4\text{Br}_4$ nanobelt. (c) The distance of lattice is about 4.2\AA . (d) XRD of Bi_4Br_4 flakes with the c axis coaligned normal to the sample holder under ambient condition. (e) The power-dependent nonlinear transmission of the Bi_4Br_4 -based SA. (f) Measured transmittivity transients of Bi_4Br_4 .

FIG. 3 The setup for measuring nonlinearity. (a) Schematic diagram of saturable absorption measurement. VOA: variable optical attenuators; OC: optical coupler. (b) The pump-probe measurements.

FIG. 4 Experimental setup and results of MLFL. (a) The experimental schematic diagram of ring cavity laser employing the Bi_4Br_4 -based SA. (b) Mode-locking phenomenon observed on the oscilloscope. (c) Optical spectrum. (d) The distribution of peaks in radio frequency (RF) spectrum. (e) Pulse duration of soliton. (f) The output power plotted as a function of the pump power. (g) The jitter of output power at pump power of 630 mW.

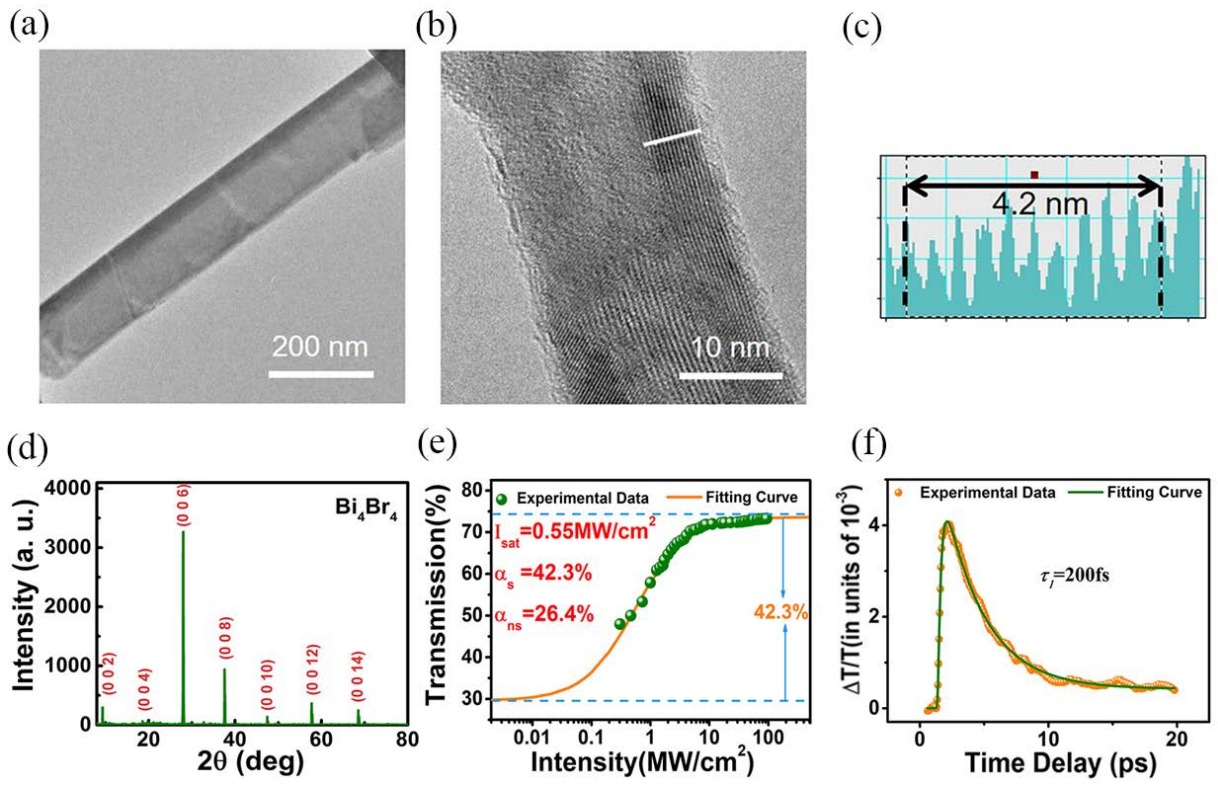
This is the author's peer reviewed, accepted manuscript. However, the online version of record will be different from this version once it has been copyedited and typeset.

PLEASE CITE THIS ARTICLE AS DOI: 10.1063/1.50077148



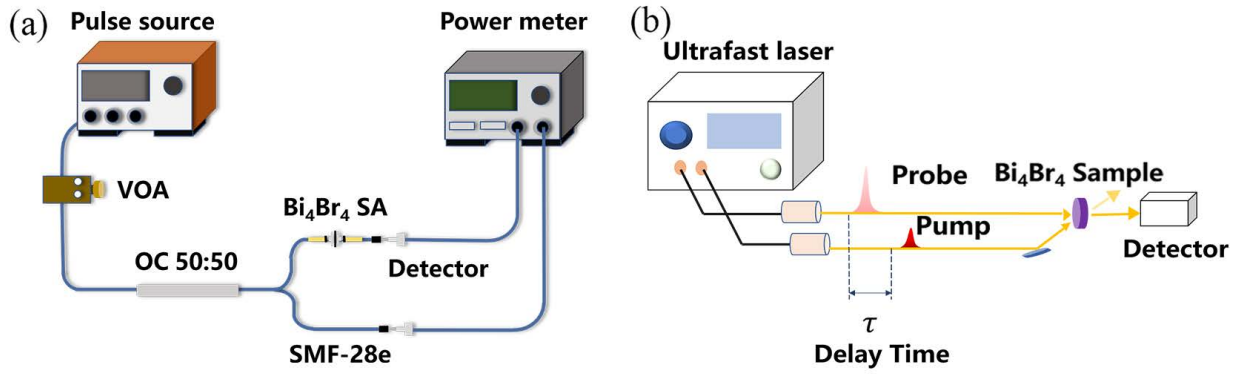
This is the author's peer reviewed, accepted manuscript. However, the online version of record will be different from this version once it has been copyedited and typeset.

PLEASE CITE THIS ARTICLE AS DOI: 10.1063/5.0077148



This is the author's peer reviewed, accepted manuscript. However, the online version of record will be different from this version once it has been copyedited and typeset.

PLEASE CITE THIS ARTICLE AS DOI: 10.1063/5.0077148



This is the author's peer reviewed, accepted manuscript. However, the online version of record will be different from this version once it has been copyedited and typeset.

PLEASE CITE THIS ARTICLE AS DOI: 10.1063/5.0077148

